RESEARCH

Quintessence scalar field and cosmological constant: dynamics of a multi-component dark energy model

Prasanta Sahoo[1,2] · Nandan Roy[2] · Himadri Shekhar Mondal[1]

Abstract

This study explores the dynamics and phase-space behavior of a multi-component dark energy model, where the dark sector consists of a minimally coupled canonical scalar field and the cosmological constant, using a dynamical system analysis setup for various types of potential for which a general parameterization of the scalar field potentials has been considered. Several fixed points with different cosmological behaviors have been identified. A detailed stability analysis has been done and possible late-time attractors have been found. For this multi-component dark energy model, the late-time attractors are either fully dominated by the cosmological constant or represent a scenario where a combination of the scalar field and the cosmological constant dominates the universe. In this type of model, there is a possibility that the scalar field can become dynamical quite early compared to the standard era of dark energy domination. However, our analysis indicates that this early time contribution of the scalar field occurs deep in the matter-dominated era, not before the recombination era.

Keywords Dark energy · Quintessence · Early dark energy · Dynamical system analysis

Contents

✉ Nandan Roy
    nandan.roy@mahidol.ac.th

    Prasanta Sahoo
    prasantmath123@yahoo.com

    Himadri Shekhar Mondal
    himumath100@gmail.com

[1] Midnapore College (Autonomous), Midnapore, West Bengal 721101, India

[2] NAS, Centre for Theoretical Physics & Natural Philosophy, Mahidol University Nakhonsawan Campus, Phayuha Khiri, Nakhon Sawan 60130, Thailand

Springer

1 Introduction

Over two decades, various cosmological observations have confirmed the ongoing accelerated expansion of the universe [1–5], yet the cause of it remains unknown. In the standard model of cosmology, we consider the accelerated expansion to be driven by the cosmological constant [6], which is consistent with current cosmological observations. However, it faces several challenges from both theoretical and observational perspectives, despite its significant achievements.

In addition to theoretical issues such as the cosmological constant problem and the fine-tuning problem, recent precision cosmological data have revealed a significant statistical discrepancy in the estimation of the Hubble parameter (H_0) between early-time and late-time observations. This discrepancy presents an additional challenge to the cosmological constant. Early universe measurements (e.g., CMB Planck [7], BAO [8, 9], BBN [10], DES [11–13]) estimate $H_0 \approx (67.0 - 68.5)$ km/s/Mpc. In contrast, late-time measurements (e.g. SH0ES [14] and H0LiCOW [15]) using time-delay cosmography find $H_0 = (74.03 \pm 1.42)$ km/s/Mpc. This $\simeq 5.3\sigma$ discrepancy [16] hints towards new physics beyond ΛCDM in the dark energy sector.

Various dynamical dark-energy models have been suggested as alternatives for the cosmological constant [17, 18]. In dynamical dark energy models the equation of state of the dark energy changes over time [19–27]. These models include but are not limited to quintessence, k-essence, and phantom-type scalar field models, where generally a scalar field is coupled with the matter minimally or non-minimally with a associated potential which can generate sufficient negative pressure to drive the accelerated expansion of the universe. Recent observations from DESI collaboration [28, 29] and other literature [30–33] have pointed towards the evidence for the dynamical nature of the dark energy over the cosmological constant.

The unknown nature of dark energy leads to the question of whether the dark sector consists of a single or multiple components. Recent literature [27, 34–37] also shows that the multi-component nature of the dark energy sector might be more preferable by current observations than the cosmological constant. Current observations also suggest that the equation of state of the scalar field might have a phantom barrier ($w_\phi = -1$) crossing in the recent past [28, 30, 31]. In [36, 38] it has been argued

that there exists a no-go theorem which prohibits a dark energy model with a single degree of freedom to cross the phantom barrier. A multi-component model of dark energy is needed for the successful phantom barrier crossing. In these types of multi-component models, the dark sector is considered to consist of a cosmological constant together with other dark energy components like a scalar field [34] or a fluid [35], or to be composed of multi-scalar fields [27]. In [34] a multi-component dark energy model has been proposed with a phantom scalar field and a cosmological constant, in [35] cosmological constant is considered with a fluid as dark energy and in [27] a generic form of the quintom model has been considered with quintessence and a phantom field as the component of dark energy. In addition, all these works suggest that multi-component models fit the data better than single component models and can significantly reduce Hubble tension compared to the Λ CDM model.

One can study the phenomenology of these multi-component dark energy models by comparing them against the state of the art cosmological observations. One can also use the powerful techniques of dynamical system analysis to investigate the phase-space behavior of these models without finding an exact solution. Dynamical system analysis is particularly useful when we are interested in the asymptotic behaviour of the system. Since these models have multiple components, it is crucial to understand their late-time behavior to identify which component might dominate the universe as the late-time attractor. In this paper, we use dynamical system analysis to investigate a multi-component dark energy model where the dark sector comprises a minimally coupled canonical scalar field, known as a quintessence field, and a cosmological constant. Our primary goal is to examine this composite model's phase space behaviour and dynamics using the dynamical systems approach. By applying appropriate variable transformations, we convert the system of equations into a set of autonomous equations. Subsequently, these equations are recast in polar form to facilitate mathematical handling. We have considered a parameterization of the scalar field potential that can incorporate various forms of potential to keep our analysis as general as possible since there is no consensus on the choice for the form of the scalar field potential. A detailed stability analysis of the system is presented. Additionally, we explore the dynamics of this model by numerically solving it, revealing the possibility of early time contribution of the scalar field.

The manuscript is structured as follows. In Section II, we cover the mathematical setup of the model. Section III forms the autonomous system, which is then transformed into polar form in Section IV. Section V provides a detailed stability analysis of the system. In Section VI, we numerically investigated the evolution of the model for different classes of potentials. Finally, in Section VII, we summarise and conclude our findings.

2 Mathematical background

In a spatially flat universe described by the standard FLRW metric which includes relativistic components, matter components, a minimally coupled canonical scalar field known as the quintessence field, and the cosmological constant; the Friedmann

equations can be expressed as follows:

$$H^2 = \frac{\kappa^2}{3} \left(\rho_m + \rho_r + \rho_\phi + \rho_\Lambda \right), \tag{1}$$

$$\dot{H} = -\frac{\kappa^2}{2} \sum_i (p_i + \rho_i). \tag{2}$$

Here, $\kappa^2 = 8\pi G$, with $H = \dot{a}/a$ denoting the Hubble parameter and $a(t)$ representing the scale factor. The terms $p_\phi = \frac{1}{2}\dot{\phi}^2 + V(\phi)$ and $\rho_\phi = \frac{1}{2}\dot{\phi}^2 - V(\phi)$ correspond to the pressure and energy density of the scalar field. The subscripts m, r, ϕ, and Λ refer to matter, radiation, quintessence, and the cosmological constant, respectively. The pressure p_i and the energy density ρ_i for each species i, namely m, r, ϕ, and Λ, are interrelated through the relation $p_i = w_i \rho_i$, where

$$w_i = \begin{cases} \frac{1}{3}, & \text{for relativistic matter} \\ 0, & \text{for non-relativistic matter} \\ -1, & \text{for } \Lambda. \end{cases}$$

The Klein-Gordon equation for the scalar field and the continuity equations, respectively, can be expressed as follows:

$$\ddot{\phi} + 3H\dot{\phi} + \frac{dV(\phi)}{d\phi} = 0, \tag{3}$$

$$\dot{\rho}_i = -3H(p_i + \rho_i), \quad \forall \ i = m, r, \phi, \Lambda. \tag{4}$$

The density parameter for a given species 'i' is expressed as $\Omega_i = \frac{\kappa^2 \rho_i}{3H^2}$. Consequently, the Friedmann constraint can be written as,

$$\Omega_m + \Omega_r + \Omega_\phi + \Omega_\Lambda = 1. \tag{5}$$

3 The dynamical system

To understand the phase-space behavior of the system, one needs to introduce a new set of dimensionless variables to write it as an autonomous system. Here we consider the following set of dimensionless transformations:

$$x^2 = \frac{\kappa^2 \dot{\phi}^2}{6H^2}, \quad y^2 = \frac{\kappa^2 V(\phi)}{3H^2},$$

$$\lambda = -\frac{1}{\kappa V} \frac{dV(\phi)}{d\phi}, \Gamma = \frac{V \frac{d^2 V}{d\phi^2}}{\left(\frac{dV}{d\phi} \right)^2}. \tag{6}$$

With the help of the above transformations, the system can be reduced to a set of autonomous equations;

$$x' = -3x + \sqrt{\frac{3}{2}}\lambda y^2 + \frac{1}{2}x\left(6x^2 + 3\Omega_m + 4\Omega_r\right), \tag{7a}$$

$$y' = -\sqrt{\frac{3}{2}}\lambda xy + \frac{1}{2}y\left(6x^2 + 3\Omega_m + 4\Omega_r\right), \tag{7b}$$

$$\Omega_m' = \Omega_m\left(-3 + 6x^2 + 3\Omega_m + 4\Omega_r\right), \tag{7c}$$

$$\Omega_r' = \Omega_r\left(-4 + 6x^2 + 3\Omega_m + 4\Omega_r\right), \tag{7d}$$

$$\lambda' = -\sqrt{6}x(\Gamma - 1)\lambda^2 = -\sqrt{6}xf. \tag{7e}$$

Here, the derivatives are with respect to $N = ln\left(\frac{a}{a_0}\right)$ and $f = (\Gamma - 1)\lambda^2$, where a_0 is the present value of the scale factor. In such a scenario, the total Equation of State (EoS) can be written as

$$\omega_{tot} \equiv \frac{p_{tot}}{\rho_{tot}} = -1 + 2x^2 + \Omega_m + \frac{4}{3}\Omega_r. \tag{8}$$

The system of equations given in Eq.(7) cannot be a closed system due to the arbitrariness of the form of the scalar field potential $V(\phi)$. To close the system, one needs to find f as a function of variables x, y, λ. Since by definition f contains the derivative of the potential, the form of it will depend only on the choice of the potential. Since there is a lack of consensus on the form of the potential of the scalar field a wide variety of potentials has been used in the literature to study these models.

In one approach, a specific potential is selected, determining the corresponding form of f. This method has already been utilized in the literature; for examples, see [39–73]. Conversely, one can start with a specific form of f and derive the corresponding potential using the definitions of y, λ, and Γ variables as given in Eq.(6). To ensure our analysis applies to a wide class of potentials, we adopt the form $f = \alpha_0 + \alpha_1\lambda + \alpha_2\lambda^2$, where α_0, α_1, and α_2 are real-valued parameters. This particular parametrisation of f was first proposed in [74]. Different choices of the α_0, α_1 and α_2 parameters will correspond to different classes of potentials. In Table-1, we list eight distinct classes of potentials, each corresponding to different choices of the α parameters. The classification was made based on whether certain α parameters are zero or not. This approach has been taken to facilitate our analysis for a wide class of potentials in a single setup. A similar approach, but for a different choice of dynamical variables, has also been used in [75]. Within the potentials listed in Table-1, V_3 and V_8 has been already studied in [76] and [77] respectively for early time solutions. Whereas in [78] dynamical system analysis for V_7 has been studied for the quintessence field.

Table 1 A list of various classes of potentials based on the different choices for the α parameters. Here A and B are integration constants

Label	Structure of f	Potential $V(\phi)$
V_1	$\alpha_0 \neq 0, \alpha_1 \neq 0, \alpha_2 \neq 0$	$A \exp\left[\dfrac{\alpha_1 k\phi - 2\log\left(\cosh\left(\frac{1}{2}\sqrt{\alpha_1^2 - 4\alpha_0\alpha_2}k(\phi+B)\right)\right)}{2\alpha_2}\right]$
V_2	$\alpha_0 = 0, \alpha_1 \neq 0, \alpha_2 \neq 0$	$A\left(e^{\alpha_1 k\phi}\right)^{\frac{1}{\alpha_2}}\left(\alpha_1\alpha_2 k\left(e^{\alpha_1 k\phi} + \alpha_2 e^{\alpha_1 Ak}\right)\right)^{-\frac{1}{\alpha_2}}$
V_3	$\alpha_0 \neq 0, \alpha_1 = 0, \alpha_2 \neq 0$	$A\cos^{-\frac{1}{\alpha_2}}\left(\sqrt{\alpha_0\alpha_2}k(\phi+B)\right)$
V_4	$\alpha_0 \neq 0, \alpha_1 \neq 0, \alpha_2 = 0$	$A \exp\left[\dfrac{\alpha_0 k^2\phi - c_1 e^{-k\alpha_1\phi}}{\alpha_1 k}\right]$
V_5	$\alpha_0 \neq 0, \alpha_1 = 0, \alpha_2 = 0$	$A \exp\left[\frac{1}{2}\alpha_0 k^2\phi^2 + B\phi\right]$
V_6	$\alpha_0 = 0, \alpha_1 \neq 0, \alpha_2 = 0$	$A \exp\left[-\dfrac{B e^{-k\alpha_1\phi}}{\alpha_1 k}\right]$
V_7	$\alpha_0 = 0, \alpha_1 = 0, \alpha_2 \neq 0$	$A\left(\alpha_2\phi + B\right)^{-\frac{1}{\alpha_2}}$
V_8	$\alpha_0 = 0, \alpha_1 = 0, \alpha_2 = 0$	$A e^{B\phi}$

4 Representation of the dynamical system in polar form

The use of polar coordinates to study the cosmological system is often useful, as shown in [74, 75, 79] because the new variables are directly related to the cosmological parameters and the mathematical handling of the system becomes easier. To transform the system of equations Eq.(7) into polar form, we use the transformation $x = r\cos\theta$ and $y = r\sin\theta$, where $r^2 = x^2 + y^2 = \Omega_\phi$. With the above choice, the system of equations reduces to

$$r' = \frac{r}{2}\left(-3 - 3\cos(2\theta) + 6r^2\cos^2\theta + 3\Omega_m + 4\Omega_r\right), \tag{9a}$$

$$\theta' = \frac{1}{2}\sin\theta\left(6\cos\theta - \sqrt{6}\lambda r\right), \tag{9b}$$

$$\Omega_m' = \Omega_m\left(-3 + 6r^2\cos^2\theta + 3\Omega_m + 4\Omega_r\right), \tag{9c}$$

$$\Omega_r' = \Omega_r\left(-4 + 6r^2\cos^2\theta + 3\Omega_m + 4\Omega_r\right), \tag{9d}$$

$$\lambda' = -\sqrt{6}r\cos\theta\left(\alpha_0 + \alpha_1\lambda + \alpha_2\lambda^2\right). \tag{9e}$$

In addition, the Friedmann constraint given in Eq.(5) takes the following form

$$r^2 + \Omega_m + \Omega_r + \Omega_\Lambda = 1. \tag{10}$$

The total equation of state and the equation of state of the scalar field can be represented in the polar form as follows,

$$\omega_{tot} = -1 + 2r^2 cos^2\theta + \Omega_m + \frac{4}{3}\Omega_r, \tag{11}$$

$$\omega_\phi \equiv \frac{p_\phi}{\rho_\phi} = cos\,2\theta. \tag{12}$$

5 Stability analysis

The equilibrium points of the system of equations given in Eq.(9) are listed in Table-2, while the eigenvalues corresponding to these points are presented in Table-3. The equilibrium points are calculated by solving the simultaneous system of equations: $r^{'} = 0$, $\theta^{'} = 0$, $\Omega_m^{'} = 0$, $\Omega_r^{'} = 0$, and $\lambda^{'} = 0$. The existence of equilibrium points for the corresponding potentials is also given in the last column of Table-2. The values for the cosmological parameters, such as the deceleration parameter, the equation of state (EoS) of the scalar field, and the total EoS for each fixed point, are provided in Table-4.

In this context, the subscript 'c' is used to denote the equilibrium points $(r_c, \theta_c, \Omega_{mc}, \Omega_{rc}, \lambda_c)$. Subsequently, we analyze the stability of these equilibrium points by categorizing them according to the different epochs of the universe they represent.

5.1 Radiation dominated era

The equilibrium points indicating the radiation domination era are characterised by $\Omega_{rc} = 1$ and represented by 'r' which are of the nonisolated type. For all the equilibrium points of this era, the corresponding Jacobian matrix has two different sets of eigenvalues depending on whether $\theta_c = n\pi$ or $\theta_c = n\pi \pm \frac{\pi}{2}$. In both cases, the Jacobian matrix has both positive and negative eigenvalues. So, these equilibrium points are saddle-like in nature and exist for all potentials ($V_1 - V_8$) listed in Table-1. From Table-4 it can be seen as expected that at these equilibrium points the universe is decelerating, and $w_{tot} = 1/3$.

5.2 Matter dominated era

The equilibrium points indicating the matter dominated era are defined by $\Omega_{mc} = 1$, and are denoted by 'm'. The Jacobian matrix, corresponding to any equilibrium point during this era, exhibits two distinct sets of eigenvalues depending on whether $\theta_c = n\pi$ or $\theta_c = n\pi \pm \frac{\pi}{2}$. For each $n \in \mathbb{Z}$, the equilibrium points during this period are categorized as saddle points due to the presence of both positive and negative

Table 2 The list of equilibrium points for the system of equations given in Eq. (9). The complete expressions of $A_\pm$, $B_\pm$, $C_\pm$, $D_\pm E_\pm$ are given in Appendix-1. The last column of the table shows the classes of potentials for which the fixed points exist

Equilibrium points	r_c	θ_c	Ω_{mc}	Ω_{rc}	λ_c	Potentials
r	0	$\frac{n\pi}{2}$	0	1	λ	$V_1 - V_8$
m	0	$\frac{n\pi}{2}$	1	0	λ	$V_1 - V_8$
$e1$	1	$n\pi$	0	0	0	$V_2, V_6 - V_8$
$e2$	1	$n\pi \pm \frac{\pi}{2}$	0	0	0	$V_1 - V_8$
$e3$	1	$n\pi$	0	0	$A\pm$	$V_1 - V_3, V_7$
$e4\pm$	1	$n\pi \pm \cos^{-1}\left(\frac{A\pm}{\sqrt{6}}\right)$	0	0	$A\pm$	$V_1 - V_3, V_7$
c	0	$\frac{n\pi}{2}$	0	0	λ	$V_1 - V_8$
$er1\pm$	$2E\pm$	$2n\pi \pm \cos^{-1}\left(\sqrt{\frac{2}{3}}\right)$	0	$B\pm$	$A\mp$	V_1, V_3
$er2\pm$	$-2E\pm$	$(2n+1)\pi \pm \cos^{-1}\left(-\sqrt{\frac{2}{3}}\right)$	0	$B\pm$	$A\mp$	V_1, V_3
$er3\pm$	$2E\pm$	$2n\pi \pm \cos^{-1}\left(\sqrt{\frac{2}{3}}\right)$	0	$1 - 4E\pm^2$	$\frac{1}{E\pm}$	V_1, V_3
$er4\pm$	$-2E\pm$	$(2n+1)\pi \pm \cos^{-1}\left(-\sqrt{\frac{2}{3}}\right)$	0	$1 - 4E\pm^2$	$\frac{1}{E\pm}$	V_1, V_3
$er5\pm$	$\pm\frac{2\alpha_2}{\alpha_1}$	$\left(n\pi \pm \cos^{-1}\left(\pm\sqrt{\frac{2}{3}}\right)\right)$	0	$1 - \frac{4\alpha_2^2}{\alpha_1^2}$	$-\frac{\alpha_1}{\alpha_2}$	V_2
$er6\pm$	$\pm\frac{2\alpha_1}{\alpha_0}$	$\left(n\pi \pm \cos^{-1}\left(\pm\sqrt{\frac{2}{3}}\right)\right)$	0	$1 - \frac{4\alpha_1^2}{\alpha_0^2}$	$-\frac{\alpha_0}{\alpha_1}$	V_4
$em1\pm$	$\sqrt{3}E\pm$	$2n\pi \pm \frac{\pi}{4}$	$C\pm$	0	$A\mp$	V_1, V_3
$em2\pm$	$-\sqrt{3}E\pm$	$2n\pi \pm \frac{3\pi}{4}$	$C\pm$	0	$A\mp$	V_1, V_3
$em3\pm$	$\pm\sqrt{3}E\pm$	$n\pi \pm \frac{\pi}{4}$	$1 - 3E\pm^2$	0	$\frac{1}{E\pm}$	V_1, V_3

Table 2 continued

Equilibrium points	r_c	θ_c	Ω_{mc}	Ω_{rc}	λ_c	Potentials
em4	$\frac{\sqrt{3}\alpha_2}{\alpha_1}$	$2n\pi \pm \frac{\pi}{4}$	$1 - \frac{3\alpha_2^2}{\alpha_1^2}$	0	$-\frac{\alpha_1}{\alpha_2}$	V_2
em5	$-\frac{\sqrt{3}\alpha_2}{\alpha_1}$	$2n\pi \pm \frac{3\pi}{4}$	$1 - \frac{3\alpha_2^2}{\alpha_1^2}$	0	$-\frac{\alpha_1}{\alpha_2}$	V_2
em6	$\frac{\sqrt{3}\alpha_1}{\alpha_0}$	$2n\pi \pm \frac{\pi}{4}$	$1 - \frac{3\alpha_1^2}{\alpha_0^2}$	0	$-\frac{\alpha_0}{\alpha_1}$	V_4
em7	$-\frac{\sqrt{3}\alpha_1}{\alpha_0}$	$2n\pi \pm \frac{3\pi}{4}$	$1 - \frac{3\alpha_1^2}{\alpha_0^2}$	0	$-\frac{\alpha_0}{\alpha_1}$	V_4
ec1	r	$n\pi \pm \frac{\pi}{2}$	0	0	0	$V_1 - V_8$
ec2±	$\pm\frac{1}{\sqrt{2}}E \pm D\mp$	$n\pi, 2n\pi \pm \cos^{-1}\left(\frac{D\mp}{2\sqrt{3}}\right)$	0	0	$A\mp$	V_1, V_3

Table 3 The list of eigenvalues of the equilibrium points given in Table-2. For the fixed points $er3_\pm, er4_\pm, em3_\pm$ the analytical forms of the eigenvalues are complicated and hence not included in the table. These eigenvalues can be computed for some particular choices of α parameters, see the text for more details

Equilibrium points	Eigenvalues
r	$4, 3, -1, 1, 0$ for $\theta = n\pi$;
	$4, -3, 2, 1, 0$ for $\theta = n\pi \pm \frac{\pi}{2}$
m	$3, 3, -\frac{3}{2}, -1, 0$ for $\theta = n\pi$;
	$-3, 3, \frac{3}{2}, -1, 0$ for $\theta = n\pi \pm \frac{\pi}{2}$
$e1$	$6, 3, 3, 2, -\sqrt{6}\alpha_1$, for even n;
	$6, 3, 3, 2, +\sqrt{6}\alpha_1$, for odd n
$e2$	$-4, -3, 0, \frac{1}{2}\left(-3 + \sqrt{9 - 12\alpha_0}\right), \frac{1}{2}\left(-3 - \sqrt{9 - 12\alpha_0}\right)$
$e3$	$2, 3, 6, \mp\sqrt{6}\sqrt{\alpha_1^2 - 4\alpha_0\alpha_2}, 3 - \sqrt{\frac{3}{2}}A_\pm$, for even n;
	$2, 3, 6, \pm\sqrt{6}\sqrt{\alpha_1^2 - 4\alpha_0\alpha_2}, 3 + \sqrt{\frac{3}{2}}A_\pm$, for odd n
$e4_\pm$	$2, 3, 6, \mp\sqrt{6}\sqrt{\alpha_1^2 - 4\alpha_0\alpha_2}, 3 - \sqrt{\frac{3}{2}}A_\pm$
c	$-4, -3, -3, 3, 0$ for $\theta = n\pi$;
	$-4, -3, -3, 0, 0$ for $\theta = n\pi \pm \frac{\pi}{2}$
$er1_\pm, er2_\pm$	$1, 4, -8\alpha_2 - 4\alpha_1 E_\pm,$
	$\frac{1}{2}\left(-1 \pm \frac{1}{\alpha_0}\sqrt{-\left(15\alpha_0^2 + 64\alpha_0\alpha_2 + 64\alpha_1\alpha_2 A_\pm\right)}\right),$
$er3_\pm, er4_\pm$	-
$er5_\pm$	$1, 4, -4\alpha_2, \frac{1}{2} \pm \left(\frac{1}{6\alpha_1}\right)\sqrt{3(3 - 8\sqrt{6})\alpha_1^2 + 96\sqrt{6}\alpha_2^2}$
$er6_\pm$	$1, 4, \frac{4\alpha_1^2}{\alpha_0}, \frac{1}{2} \pm \left(\frac{1}{6\alpha_0}\right)\sqrt{3(3 - 8\sqrt{6})\alpha_0^2 + 96\sqrt{6}\alpha_1^2}$
$em1_\pm, em2_\pm$	$-1, 3, -6\alpha_2 - 3\alpha_1 E_\pm,$
	$\frac{3}{4}\left(-1 \pm \frac{1}{\alpha_0}\sqrt{-\left(7\alpha_0^2 + 24\alpha_0\alpha_2 + 24\alpha_1\alpha_2 A_\pm\right)}\right),$
$em3_\pm$	-
$em4, em5$	$-1, 3, -3\alpha_2, \frac{3}{4}\left(-1 \pm \left(\frac{3}{4\alpha_1}\right)\sqrt{24\alpha_2^2 - 7\alpha_1^2}\right)$
$em6, em7$	$-1, 3, \frac{3\alpha_1^2}{\alpha_0}, \frac{3}{4}\left(-1 \pm \left(\frac{3}{4\alpha_0}\right)\sqrt{24\alpha_1^2 - 7\alpha_0^2}\right)$
$ec1$	$-4, -3, 0, \frac{1}{2}\left(-3 \pm \sqrt{9 - 12\alpha_0 r_c^2}\right)$
$ec2_\pm$	$2, 3, 6, 3\mp\frac{\sqrt{3}}{2}\sqrt{-\frac{2\alpha_0}{\alpha_2} - \frac{2\alpha_1}{\alpha_2}A_\mp},$
	$\pm\frac{\sqrt{3}\alpha_2}{\alpha_0}A_\pm\sqrt{\alpha_1^2 - 4\alpha_0\alpha_2}\sqrt{-\frac{2\alpha_0}{\alpha_2} - \frac{2\alpha_1}{\alpha_2}A_\mp}$, for even n and $sin\theta = 0$;
	$2, 3, 6, 3 \pm \frac{\sqrt{3}}{2}\sqrt{-\frac{2\alpha_0}{\alpha_2} - \frac{2\alpha_1}{\alpha_2}A_\mp},$
	$\mp\frac{\sqrt{3}\alpha_2}{\alpha_0}A_\pm\sqrt{\alpha_1^2 - 4\alpha_0\alpha_2}\sqrt{-\frac{2\alpha_0}{\alpha_2} - \frac{2\alpha_1}{\alpha_2}A_\mp}$, for odd n and $sin\theta = 0$;
	$2\alpha_0 + \alpha_1 A_\mp, -\frac{\alpha_0}{\alpha_2} - \left(\frac{\alpha_1}{\alpha_2}\right)A_\mp, -\frac{1}{\alpha_2}(\alpha_0 + 3\alpha_2) - \left(\frac{\alpha_1}{\alpha_2}\right)A_\mp,$
	$-\frac{1}{\alpha_2}(\alpha_0 + 4\alpha_2) - \left(\frac{\alpha_1}{\alpha_2}\right)A_\mp, -\frac{1}{2\alpha_2}(\alpha_0 + 6\alpha_2) - \left(\frac{\alpha_1}{2\alpha_2}\right)A_\mp$, for $cos\theta = \frac{D_\mp}{2\sqrt{3}}$

Table 4 The values of cosmological parameters for the equilibrium points given in Table-2

Equilibrium points	q	ω_ϕ	ω_{tot}
r	1	1 for $\theta = n\pi$ -1 for $\theta = n\pi \pm \frac{\pi}{2}$	$\frac{1}{3}$
m	$\frac{1}{2}$	1 for $\theta = n\pi$; -1 for $\theta = n\pi \pm \frac{\pi}{2}$	0
$e1, e3, e4\pm$	2	1	1
$e2$	-1	-1	-1
c	-1	1 for $\theta = n\pi$; -1 for $\theta = n\pi \pm \frac{\pi}{2}$	-1
$er1\pm, er2\pm,$	$\dfrac{\alpha_0^2 + 16\alpha_2\alpha_0 + 8\left(\sqrt{\alpha_1^2 - 4\alpha_0\alpha_2} - \alpha_1\right)\alpha_1}{\alpha_0^2},$ for $er+$	$\frac{1}{3}$	$\frac{1}{3}$
$er3\pm, er4\pm$	$\dfrac{\alpha_0^2 + 16\alpha_2\alpha_0 - 8\alpha_1\left(\sqrt{\alpha_1^2 - 4\alpha_0\alpha_2} + \alpha_1\right)}{\alpha_0^2},$ for $er-$		
$er5\pm, er6\pm$	$1 - \dfrac{16\alpha_1^2}{\alpha_0^2}$, for $er5\pm$; $1 - \dfrac{16\alpha_2^2}{\alpha_1^2}$, for $er6\pm$	$\frac{1}{3}$	$\frac{1}{3}$
$em1\pm,$	$\dfrac{\alpha_0^2 + 18\alpha_2\alpha_0 + 9\left(\sqrt{\alpha_1^2 - 4\alpha_0\alpha_2} - \alpha_1\right)\alpha_1}{2\alpha_0^2},$ for $em+$	$\frac{1}{3}$	$\frac{1}{3}$
$em2\pm, em3\pm$	$\dfrac{\alpha_0^2 + 18\alpha_2\alpha_0 - 9\alpha_1\left(\sqrt{\alpha_1^2 - 4\alpha_0\alpha_2} + \alpha_1\right)}{2\alpha_0^2},$ for $em-$		

Table 4 continued

Equilibrium points	q	ω_ϕ	ω_{tot}
$em4, em5$	$\frac{1}{2}-\frac{9\alpha_2^2}{\alpha_1^2}$	0	0
$em6, em7$	$\frac{1}{2}-\frac{9\alpha_1^2}{\alpha_0^2}$	0	0
$ec1$	-1	-1	-1
$ec2\pm$	-4, for $\theta = n\pi$;	1, for $\theta = n\pi$;	1, for $\theta = n\pi$;

For $ec2\pm$:

q:

$$\frac{2(\alpha_0-2\alpha_2)\alpha_2-\alpha_1\left(\sqrt{\alpha_1^2-4\alpha_0\alpha_2}+\alpha_1\right)}{4\alpha_2^2},$$
for $r_c = \pm\frac{1}{\sqrt{2}}E+D_-$

$$\frac{\left(\sqrt{\alpha_1^2-4\alpha_0\alpha_2}-\alpha_1\right)\alpha_1+2\alpha_2(\alpha_0-2\alpha_2)}{4\alpha_2^2},$$
for $r_c = \pm\frac{1}{\sqrt{2}}E-D_+$

ω_ϕ:

$$\frac{\alpha_1\left(\sqrt{\alpha_1^2-4\alpha_0\alpha_2+\alpha_1}\right)-2\alpha_2(\alpha_0+3\alpha_2)}{6\alpha_2^2},$$
for $r_c = \pm\frac{1}{\sqrt{2}}E+D_-$

$$\frac{\alpha_1\left(\left(\sqrt{\alpha_1^2-4\alpha_0\alpha_2+\alpha_1}\right)-2\alpha_2(\alpha_0+3\alpha_2)\right)}{6\alpha_2^2},$$
for $r_c = \pm\frac{1}{\sqrt{2}}E-D_+$

ω_{tot}:

$$\frac{\alpha_1^2-\sqrt{\alpha_1^2-4\alpha_0\alpha_2\alpha_1}-2\alpha_2(\alpha_0+3\alpha_2)}{6\alpha_2^2},$$
for $r_c = \pm\frac{1}{\sqrt{2}}E+D_-$

$$\frac{\alpha_1^2-\sqrt{\alpha_1^2-4\alpha_0\alpha_2\alpha_1}-2\alpha_2(\alpha_0+3\alpha_2)}{6\alpha_2^2},$$
for $r_c = \pm\frac{1}{\sqrt{2}}E-D_+$

eigenvalues corresponding to these fixed points. These equilibrium points for the matter domination era are present for all potentials $V_1 - V_8$ and represent a decelerating universe with $w_{tot} = 0$.

5.3 Scalar field dominated era

For the equilibrium points in the scalar field domination era, we have $r_c = 1$. In this case, the equilibrium points are given by, $e1$ - $e4_\pm$, The eigenvalues of the Jacobian matrix at '$e1$' depend on α_1. But, for the existence of positive eigenvalues of the Jacobian matrix at '$e1$', the equilibrium points given by '$e1$' are unstable and exist for the potentials V_2 and $V_6 - V_8$. These equilibrium points represent a decelerating universe with $w_{tot} = 1$.

The equilibrium points indicated by '$e2$' are nonhyperbolic, characterised by a zero eigenvalue. These fixed points may be stable within the parameter range $0 < \alpha_0 \le \frac{3}{4}$, as the remaining two eigenvalues can be negative. Due to their non-hyperbolic nature, linear stability analysis cannot determine their stability. Instead, stability must be assessed using center manifold theory or by numerically plotting the system's phase around the fixed point. Given that the system's dimension exceeds three, a complete phase plot is impractical; hence, phase portraits are drawn on various projected planes. If all projected phase planes depict the equilibrium point as stable, it is stable in the full space. Conversely, if any projected phase space shows instability, the equilibrium point is unstable in the entire space. For the equilibrium point '$e2$', we draw a phase plot (Fig. 1) in the (r, Ω_m) plane. This phase plot indicates that the equilibrium points specified by '$e2$' are unstable on the (r, Ω_m) plane and consequently in the full space. Those equilibrium points represent an accelerating universe with $w_\phi = w_{tot} = -1$.

The equilibrium points, labelled as '$e3$' and '$e4_\pm$', are identified for $r_c = 1$, $\Omega_{mc} = 0$, $\Omega_{rc} = 0$, and $\lambda_c = A_\pm$ (refer to Appendix: 1 for the complete form of $A_\pm$). These fixed points exist for the potentials $V_1 - V_3$ and V_7. However, the values of θ_c are not the same for these points. These equilibrium points exist when $\alpha_2 \ne 0$ and $\alpha_1^2 - 4\alpha_0\alpha_2 \ge 0$. The eigenvalues of '$e3$' are determined by whether n is even or odd, while the eigenvalues of '$e4_\pm$' are independent of n. In all cases, the Jacobian matrix evaluated at '$e3$' and '$e4_\pm$' exhibits positive eigenvalues. Consequently, the fixed points represented by '$e3$' and '$e4_\pm$' are unstable regardless of the values of n and the parameters α_0, α_1, and α_2. These fixed points represent a decelerating universe with $w_\phi = w_{tot} = 1$.

5.4 Λ - dominated era

The equilibrium points representing the cosmological constant or Λ-domination era are represented by $r_c = 0$, $\Omega_{mc} = 0$, and $\Omega_{rc} = 0$ and exist for all classes of potentials. In this case, the equilibrium points are given by 'c' in the Table-2 and they are nonisolated equilibrium points. The eigenvalues of the Jacobian matrix evaluated at 'c' depend on θ_c. For $\theta_c = n\pi$ the Jacobian matrix has a mixture of positive and negative eigenvalues, hence the fixed points in this case are saddle. On the other hand, finding the stability of the equilibrium points 'c' for $\theta_c = n\pi \pm \frac{\pi}{2}$ is more involved
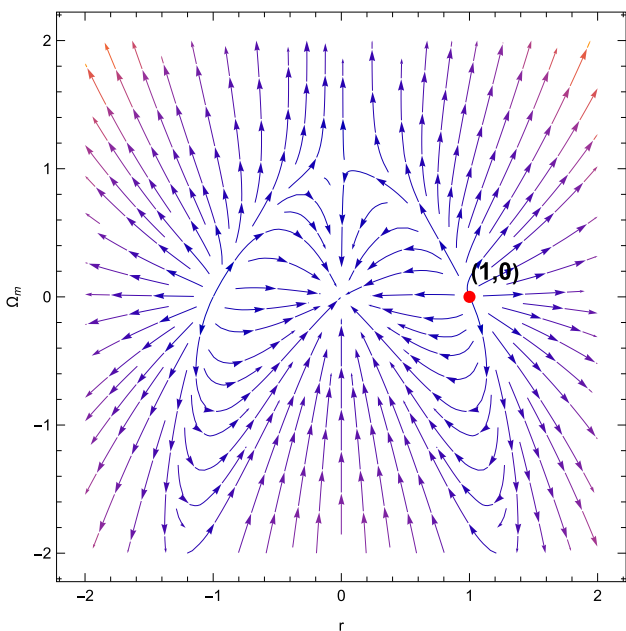
Fig. 1 Phase plot for the system of equations Eq.(9) in $(r - \Omega_m)$ plane for the fixed point, e_2

since it has two zero eigenvalues and other all negative eigenvalues. Three negative eigenvalues correspond to a 3D stable manifold, whereas the two zero eigenvalues correspond to a 2D center manifold. In general, one can use the center manifold theorem to investigate the stability of this fixed point, rather here we draw the phase plots on 3D planes. All the points in red color and the points on the lines shown in red in the projected phase spaces, as depicted in Fig. 2, represent the equilibrium point 'c' for the V_2 potential. From this figure, we can see that the fixed points given by 'c' are stable for $\theta = n\pi \pm \frac{\pi}{2}$ in all projected subspaces and hence stable in the entire 5D space. We have also checked that for the other class of potentials, the behaviour of the fixed point remains the same. These fixed points represent an accelerating universe with $w_\phi = 1$ and $w_{tot} = -1$ for $\theta = n\pi$ whereas $w_\phi = w_{tot} = -1$ for $\theta = n\pi \pm \frac{\pi}{2}$. Interestingly, in the first case, the scalar field behaves as a stiff fluid.

5.5 The era shared by scalar field and other components

In our setup, there are some specific fixed points that indicate scenarios where the energy budget is shared between the scalar field and other components.

The era shared by the scalar field and radiation

The fixed points '$er1_\pm$' to '$er6_\pm$' represent the state where the universe's energy budget is shared by radiation and the scalar field by the relation $r_c^2 + \Omega_{rc} = 1$. For each $n \in \mathbb{Z}$, the equilibrium points '$er1_\pm$', '$er2_\pm$', '$er5_\pm$', and '$er6_\pm$' exhibit posi-
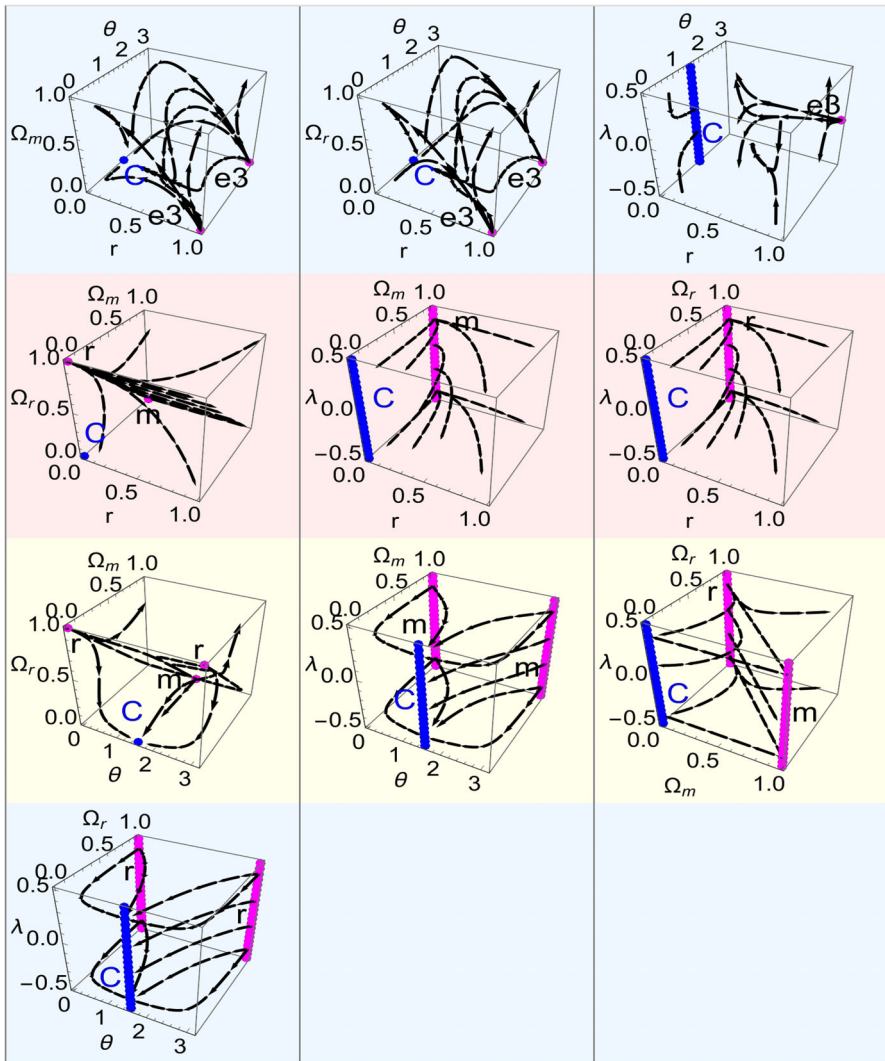
Fig. 2 Phase plots in different $3D$ projected spaces for the equilibrium point 'c' and for the potential V_2. The location of the fixed point 'c' is depicted by the blue point/line. The points/line in magenta color represents the location of the other fixed points which are unstable in nature

tive eigenvalues, making these points unstable or saddle depending on the choice of parameters $\alpha_0, \alpha_1, \alpha_2$. The eigenvalues of the Jacobian matrix at '$er3_\pm$' and '$er4_\pm$' are complicated in general, making it difficult to draw any conclusions about their stability. For these points, we evaluate the stability at specific values of α parameters. We have considered the same value of the α parameters that have been used to plot Fig. 4 and Fig. 6, for potentials V_1 and V_3 respectively. For the potential V_1 the eigenvalues at '$er3_\pm$' are 1, 4, -2.8394, and $-0.5 \pm 1.93041i$, while at '$er4_\pm$' they are -201.793, -11.2262, 10.2262, 4, and 1, indicating that these points are saddle

points. For potential V_3, the eigenvalues at '$er3_\pm$' and '$er4_\pm$' are $1, 4, -4.48$, and $-0.5 \pm 1.92544i$, showing that they are saddle points. The fixed points '$er1_\pm$' and '$er2_\pm$' exist for the potentials V_1 and V_3; '$er5_\pm$' exist for the potential V_2; and '$er6_\pm$' for potential V_4. For all possible equilibrium points in this era $w_\phi = w_{tot} = 1/3$ representing a decelerated universe.

The era shared by the scalar field and matter

For the equilibrium points in the era shared by scalar field and matter, we have $r_c^2 + \Omega_{mc} = 1$. In this case, the equilibrium points are given by '$em1_\pm$' - '$em7$'. For each $n \in \mathbb{Z}$, though the eigenvalues of the Jacobian matrix evaluated at the equilibrium points '$em1_\pm$', '$em2_\pm$' and '$em4$' - '$em7$' depend on the parameters α_0, α_1 and α_2; but it has a positive eigenvalue irrespective of α_i. So, the equilibrium points given in this era are unstable in nature. The equilibrium points '$em1_\pm$' - '$em3_\pm$' exist for the potentials V_1, V_3; '$em4$' and '$em5$' exist for the potential V_2; '$em6$' and '$em7$' exist for the potential V_4. The eigenvalues of the Jacobian matrix evaluated at the equilibrium point '$em3_\pm$' are very complicated. So, for '$em3_\pm$', we evaluate the stability similarly as the case for '$er3_\pm$' and '$er4_\pm$'. For the potential V_1 the eigenvalues at '$em3_+$' are $3, -1, -2.12955$, and $-0.75 \pm 1.97931i$, while at '$er3_-$' they are $9.06334, 3, -1, -10.5633$, and -151.345, indicating that these points are saddle points. For potential V_3, the eigenvalues at '$em3_\pm$' are $3, -1, -3.36$, and $-0.75 \pm 1.97522i$, showing that they are saddle points. The exact value of the deceleration parameter depends on α parameters for all the potentials belonging to this era. However, for all possible equilibrium points in this era $w_\phi = w_{tot} = 0$ or $1/3$ representing a decelerated universe.

The era shared by the scalar field and Λ

For the equilibrium points in the era shared by scalar field and Λ, we have $r_c^2 + \Omega_{\Lambda_c} = \Omega_{\phi_c} + \Omega_{\Lambda_c} = 1$. In this case, the equilibrium points are given by '$ec1$' and '$ec2_\pm$'. The equilibrium points given by '$ec1$' exist for all potentials $V_1 - V_8$. The nature of the equilibrium points given by '$ec1$' depends on the parameter α_0. If $0 < \alpha_0 < \frac{3}{4r_c^2}$, then the equilibrium points given by '$ec1$' are normally hyperbolic equilibrium points and the Jacobian matrix has four eigenvalues with negative real parts and one zero eigenvalue. Again, if $\alpha_0 = 0$ then the equilibrium points given by '$ec1$' are of non-hyperbolic type and the Jacobian matrix has three negative and two zero eigenvalues. To check the stability of those equilibrium points we plot the evolution of the dynamical variables r, θ, Ω_m, Ω_r and λ by solving the system numerically where the system has been perturbed from the equilibrium point '$ec1$'. This approach for finding the stability of the non-hyperbolic fixed points has been previously used in [78, 80, 81]. In Fig. 3 for example we have plotted the evolution of the system with N for the potentials V_1 (on the left column) and V_8 (on the right column) subjected to perturbations around the fixed point 'ec_1'. We can see that the evolution of the dynamical variables does not diverge but rather stays in the neighbourhood of the fixed point, indicating its stable nature. We have also checked that the qualitative behaviour of the fixed point

remains the same even for the other potentials. Thus, the fixed points given by '$ec1$' are stable for $\alpha_0 = 0$. Again, if $\alpha_0 < 0$, then the equilibrium points given by '$ec1$' are non-hyperbolic type and the Jacobian matrix has a positive eigenvalue. Thus, the equilibrium points given by '$ec1$' are stable for $0 \leq \alpha_0 \leq \frac{3}{4r_c^2}$, where $0 \leq r_c \leq 1$ and unstable for $\alpha_0 < 0$. These fixed points represent an accelerating universe with $w_\phi = w_{tot} = -1$.

The equilibrium points '$ec2_\pm$' are defined by $r_c = \pm \frac{1}{\sqrt{2}} E_\pm D_\mp$, $\Omega_{mc} = 0$, $\Omega_{rc} = 0$, and $\lambda_c = A_\mp$ and exists for potentials V_1 and V_3. There are two distinct types of θ_c at these points: $\theta_c = n\pi$ and $\theta_c = 2n\pi \pm \cos^{-1} \frac{D_\mp}{2\sqrt{3}}$. For $\theta_c = n\pi$, the eigenvalues of the Jacobian matrix vary depending on whether n is even or odd, but some eigenvalues are always positive, hence the fixed points are unstable. For $\theta_c = 2n\pi \pm \cos^{-1} \frac{D_\mp}{2\sqrt{3}}$, the form of the eigenvalues is complicated, and it is not possible to conclude stability analytically for this fixed point for any general choice of the parameters α. Thus, stability was assessed for specific values of the parameters α_0, α_1, and α_2 that are considered for the numerical solutions shown in Fig. 1 and Fig. 3. The Jacobian matrix has at least one positive eigenvalue for our choices of the α parameters, making '$ec2_\pm$' unstable. These points also correspond to an accelerating universe.

6 Numerical investigation

In our analysis of the phase space for the current model, we observed that there is no late-time attractor completely dominated by the scalar field. The only possible late-time attractors are either completely dominated by the cosmological constant or a scenario where there is only the cosmological constant and scalar field present in the universe; the rest of the components are absent. Although there might be some epochs where the scalar field and other components coexist, represented by saddle or unstable fixed points. For example, the fixed points in Table:2 where r_c and some other components like Ω_{mc} or Ω_{rc} are non-zero. In the following, we have numerically evolved the system to investigate the evolution of the different cosmological parameters, and we will see, as expected from the fixed point analysis, that there are possibilities of some eras of the universe which are shared by the scalar field and other components of the universe much before the standard era of dark energy domination.

We have numerically solved the system of equations Eq.(9) by considering the specific initial conditions given in Table-5. In particular, except for the initial condition of λ for all potentials, the initial conditions for the other variables remain almost the same. The initial condition is set before the radiation-matter equality at $N = -10.1$, corresponding to $z \approx 22026$, deep in the radiation-dominated era. The range of α parameters and λ_{ini} for each class of potential is presented in Table-6, for which the qualitative behaviour of our analysis remains the same.

The evolution of the density parameters for various components of the universe corresponding to all the classes of potentials are shown in Fig. 4 to Fig. 11 respectively. For the classes of potentials, V_1 - V_6 one can see the scalar field contribute to the energy budget of the universe earlier than the expected dark energy domination epoch for a short period resembling EDE-like behaviour of the scalar field appearing naturally
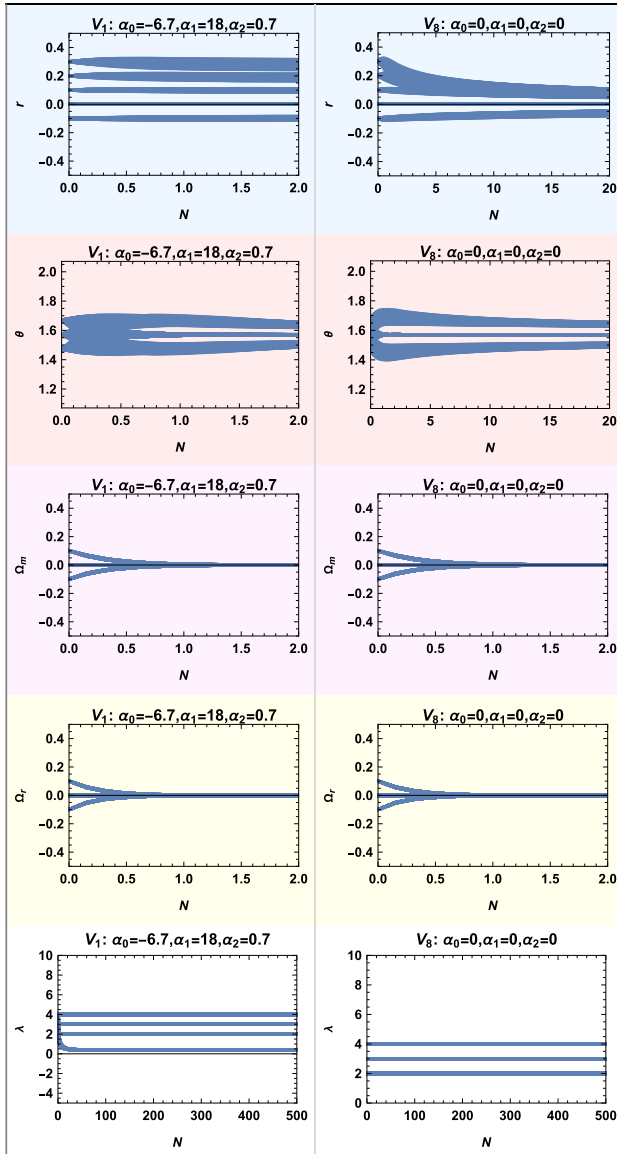
Fig. 3 Plots of the numerical solutions for each dynamical variable by considering perturbations around the equilibrium point '$ec1$'. The plots in the left column are shown for potential V_1 and on the right it is shown for the potential V_8

in the deep-matter dominated era, which is almost 10% of the total energy budget of the universe. But, at present the contribution of the scalar field is negligible for these potentials. Whereas for the classes of potentials, V_7 and V_8 also the similar behaviour of the scalar field appears naturally in the deep matter-dominated era, which is almost 10% of the total energy budget of the universe. Contrary to the previous case, for
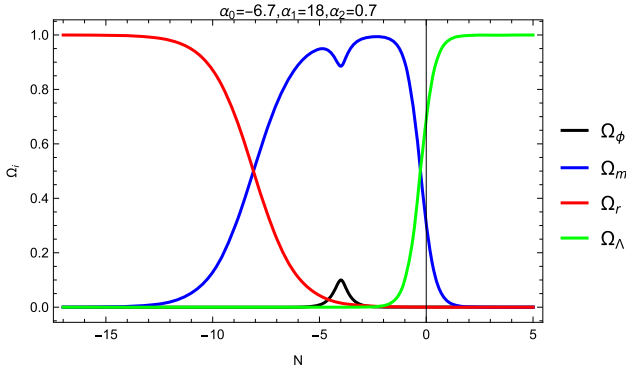
Fig. 4 Plot of the density parameters for different components of the universe for the potential V_1
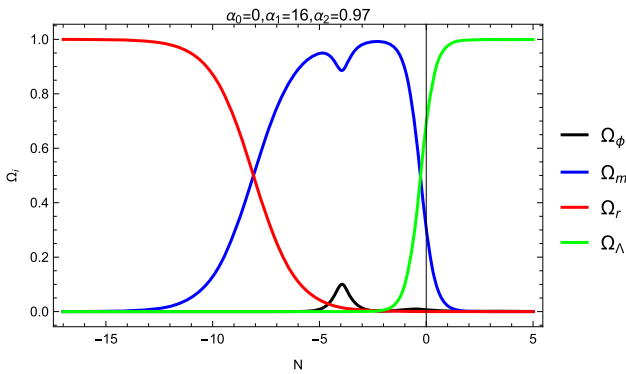
Fig. 5 Plot of the density parameters for different components of universe for the potential V_2
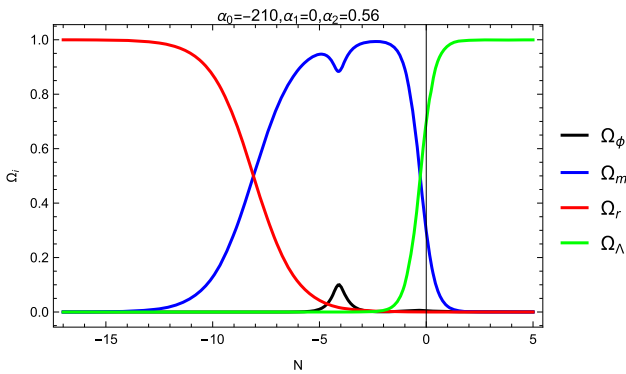

Fig. 6 Plot of the density parameters for different components of universe for the potential V_3

these two classes of potentials, at present as well as near future, the scalar field has a non-negligible contribution to the total energy budget of the universe. The redshift parameter values for matter-radiation equality and the occurrence of this behavior of the scalar field are provided in Table-6 for all classes of potentials.
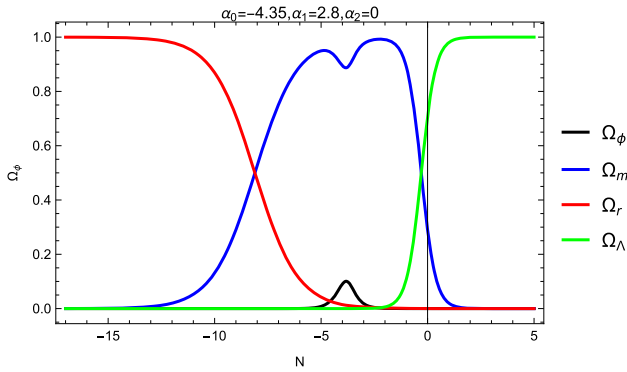
Fig. 7 Plot of the density parameters for different components of universe for the potential V_4
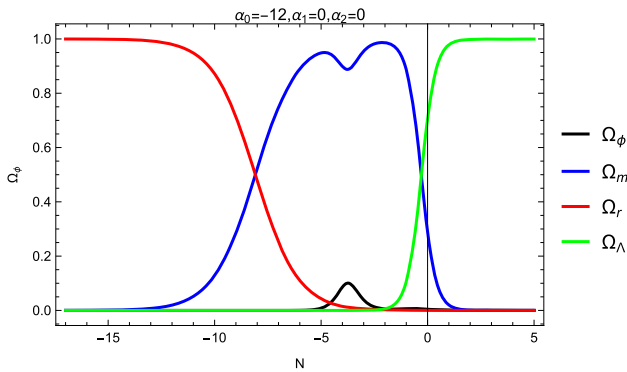

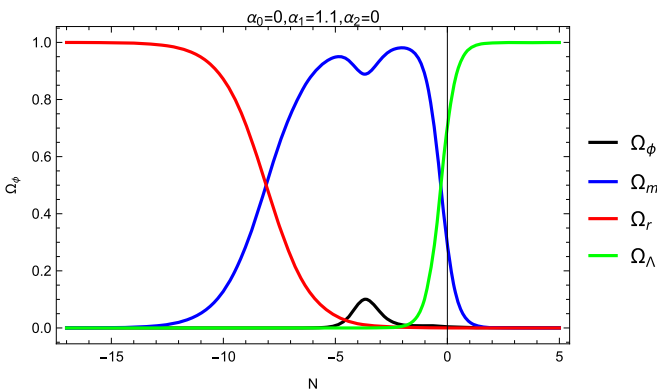**Fig. 8** Plot of the density parameters for different components of universe for the potential V_5

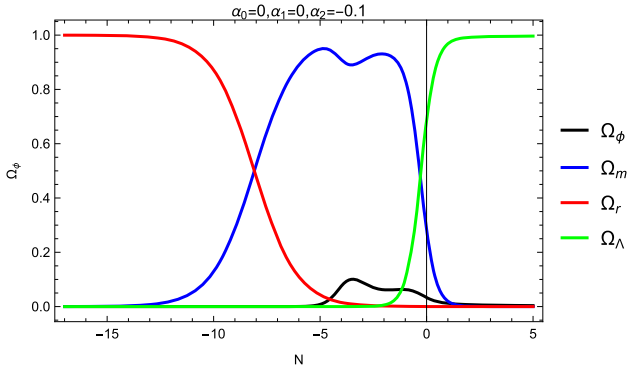**Fig. 9** Plot of the density parameters for different components of universe for the potential V_6

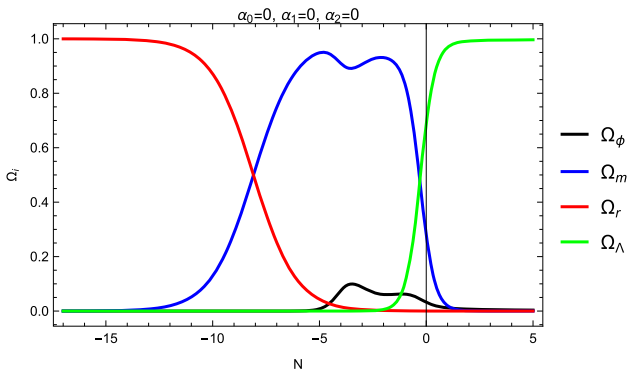**Fig. 10** Plot of the density parameters for different components of universe for the potential V_7

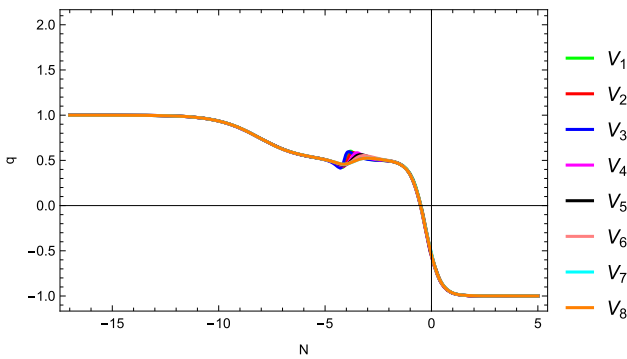**Fig. 11** Plot of the density parameters for different components of universe for the potential V_8
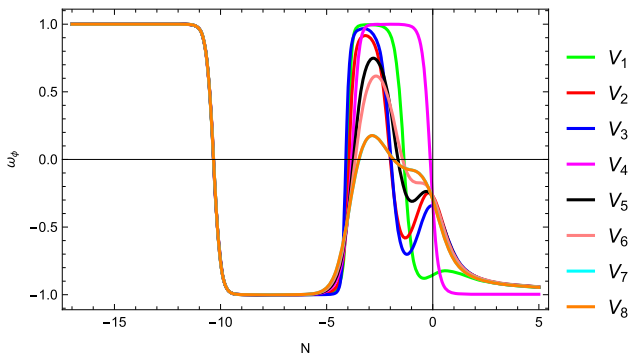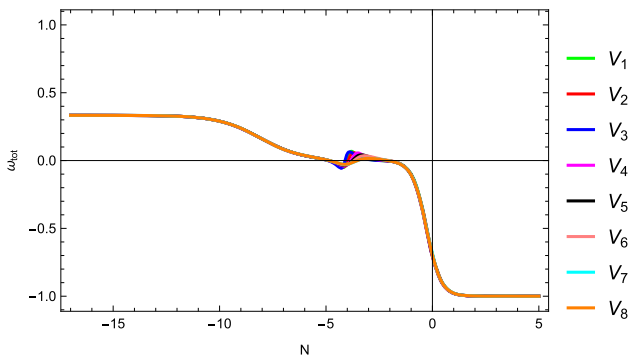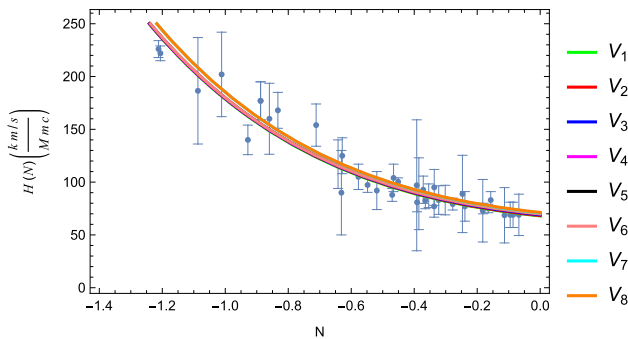

Fig. 12 Plots of the deceleration parameter with respect to different classes of potentials

Fig. 13 Plots of the equation of state for scalar field for different classes of potentials

Fig. 14 Plots of the total equation of state with respect to different classes of potentials

Fig. 15 Plot of the evaluation of the Hubble parameter $H(N)$ versus N for different classes of potentials. The data from various observations are also included for comparison

We have also plotted the evolution of different cosmological parameters like the deceleration parameter in Fig. 12, the equation of state of the scalar field in Fig. 13 and the total equation of state in Fig. 14 for all potentials. Those plots are drawn for the same values of the parameters α for which Fig. 4 to Fig. 11 are drawn. For the evolution of the deceleration parameter, one can see that its value has become negative in the recent past from positive, showing the accelerating expansion of the universe. It can

be seen that the transition of the universe from the decelerated to the accelerated phase remains smooth throughout except for the epoch where the scalar field shows early time contribution. During this epoch, the deceleration parameter shows some increments suggesting more deceleration of the universe due to the activation of the scalar field. Later, it started to decrease and become negative with time. From the plot of the EOS of the scalar field in Fig. 13 one can see that in the very early universe, the scalar field behaves like a stiff fluid with EOS $w_\phi = 1$ then it becomes $w_\phi = -1$. During the early contribution period of the scalar field, it increases and becomes positive and the scalar field does not contribute to the acceleration of the universe since $w_\phi > -1/3$ rather it was slowing down the expansion of the universe. This can also be seen from the plot of the w_{tot} in Fig. 14 since during this epoch the w_{tot} becomes positive and starts to decrease again.

In Fig. 15 we have shown the evolution of the $H(z)$ vs z for all the classes of potentials together with the observed data from different observations for comparison. Please see Section:1 for more details about the data used in this plot. It can be seen that even though the scalar field contributed during the matter-dominated era, these potentials fit the data quite well, at least during the late time evolution.

A similar approach to study the early dark energy behavior of the scalar field using dynamical system analysis was used in [76, 77]. Both works show that EDE-like behavior of the scalar field before the recombination era can be achieved, but it is subjected to a high degree of approximations. One of the advantages of our approach is that one can find EDE-like behaviour of the scalar field more generically without any approximation and the result applies to a wide class of potentials.

7 Conclusion

In this study, we explore the dynamics and phase-space characteristics of a multicomponent dark energy model. This model features a dark sector that includes a minimally coupled canonical scalar field and a cosmological constant. The equations are transformed into autonomous systems and subsequently into polar form. Since we are interested in making our analysis valid for a wide class of potentials, enabling us to study the multi-component models from a more general point of view, we have considered a parameterization for the potentials of the scalar field that helps us study a broad spectrum of potentials in a single setup.

By using dynamical system analysis, we find several fixed points that correspond to various cosmological eras together with possible late-time attractors. In this model, the late-time attractors are either completely dominated by the cosmological constant or present a scenario where both the scalar field and the cosmological constant coexist, excluding all other components.

We also investigated numerically the evolution of different cosmological parameters and compared it with the observed data. Most interestingly, our findings show the early time contribution of the scalar field occurring deep within the matter-dominated era, not near the recombination period. We also found that during this era of the scalar field, it behaves more like matter rather than dark energy, and the universe becomes more decelerated compared to the standard case. The total EOS of the universe also

Table 5 The initial values of the variables for which the numerical solution of the system of equations Eq.(9) has been obtained

Potentials	N_{ini}	r_{ini}	θ_{ini}	$\Omega_{m_{ini}}$	$\Omega_{r_{ini}}$	λ_{ini}
V_1	-10.1	$\sqrt{0.3 \times 10^{-9}}$	$tan^{-1}(-2)$	$0.118 - \frac{(r_{ini})^2}{2}$	$0.882 - \frac{(r_{ini})^2}{2}$	-2.4
V_2	-10.1	$\sqrt{0.3 \times 10^{-9}}$	$tan^{-1}(-2)$	$0.118 - \frac{(r_{ini})^2}{2}$	$0.882 - \frac{(r_{ini})^2}{2}$	-2.93
V_3	-10.1	$\sqrt{0.36 \times 10^{-9}}$	$tan^{-1}(-2)$	$0.118 - \frac{(r_{ini})^2}{2}$	$0.882 - \frac{(r_{ini})^2}{2}$	-0.64
V_4	-10.1	$\sqrt{0.3 \times 10^{-9}}$	$tan^{-1}(-2)$	$0.118 - \frac{(r_{ini})^2}{2}$	$0.882 - \frac{(r_{ini})^2}{2}$	-4.49
V_5	-10.1	$\sqrt{0.3 \times 10^{-9}}$	$tan^{-1}(-2)$	$0.118 - \frac{(r_{ini})^2}{2}$	$0.882 - \frac{(r_{ini})^2}{2}$	-5.13
V_6	-10.1	$\sqrt{0.3 \times 10^{-9}}$	$tan^{-1}(-2)$	$0.118 - \frac{(r_{ini})^2}{2}$	$0.882 - \frac{(r_{ini})^2}{2}$	-5.785
V_7	-10.1	$\sqrt{0.3 \times 10^{-9}}$	$tan^{-1}(-2)$	$0.118 - \frac{(r_{ini})^2}{2}$	$0.882 - \frac{(r_{ini})^2}{2}$	-6
V_8	-10.1	$\sqrt{0.3 \times 10^{-9}}$	$tan^{-1}(-2)$	$0.118 - \frac{(r_{ini})^2}{2}$	$0.882 - \frac{(r_{ini})^2}{2}$	-6.59

Table 6 The range of parameters and λ_{ini} for which the qualitative behavior of the numerical solution of the system of equations Eq. (9) remains unchanged

Potentials	λ_{ini}	α_0	α_1	α_2	z_{eq}	z_*
V_1	$[-2.5, -2.4]$	$[-20, -4.65]$	$[18, 20]$	$[0.4, 0.7]$	3228	54
V_2	$[-3, -2.93]$	0	$[16, 20]$	$[0.9, 1]$	3228	52
V_3	$[-0.7, -0.5]$	$[-270, -200]$	0	$[0.47, 0.8]$	3228	58
V_4	$[-4.6, -4.49]$	$[-8, -4.35]$	$[2.8, 3]$	0	3293	43
V_5	$[-5.3, -5.13]$	$[-16.5, -12]$	0	0	3228	44
V_6	$[-5.9, -5.785]$	0	$[0.9, 1.1]$	0	3228	40
V_7	$[-6.1, -5.99]$	0	0	$[-0.15, -0.1]$	3228	38
V_8	$[-6.9, -6.59]$	0	0	0	3228	31

shows a transition from negative to positive values during this epoch. We acknowledge that a comprehensive parameter estimation for the choice of α parameters using a Boltzmann code like CLASS and current cosmological data is necessary to comment more accurately on this early-time contribution of the scalar field and how it could affect the overall evaluation and structure formation of the universe. Since this study focuses on the investigation of the phase space behaviour of the model, it is beyond the scope of the current work. It will be addressed in future research.

Appendix

$$A_\pm = \frac{-\alpha_1 \pm \sqrt{\alpha_1^2 - 4\alpha_0\alpha_2}}{2\alpha_2}.$$

$$E_\mp = \frac{-\alpha_1 \pm \sqrt{\alpha_1^2 - 4\alpha_0\alpha_2}}{2\alpha_0},$$

$$B_\pm = 1 + \frac{4\alpha_2}{\alpha_0} + \frac{4\alpha_1}{\alpha_0} E_\pm,$$

$$C_\pm = 1 + \frac{3\alpha_2}{\alpha_0} + \frac{3\alpha_1}{\alpha_0} E_\pm,$$

$$D_\mp = \sqrt{-\frac{2}{\alpha_2}(\alpha_1 A_\mp + \alpha_0)}.$$

Observed data for the Hubble's parameter vs. redshift & the e-folding

Table 7 Observed data for $H(z)$ as a function of z alongside the associated value of N, with references that have been used in this study

z	$N = \ln\left(\frac{1}{1+z}\right)$	$H(z)\left(\frac{km/s}{Mpc}\right)$	Refs.	z	$N = \ln\left(\frac{1}{1+z}\right)$	$H(z)\left(\frac{km/s}{Mpc}\right)$	Refs.
0.07	−0.067	69 ± 19.6	[82]	0.4783	−0.390	80.9 ± 9	[84]
0.09	−0.086	69 ± 12	[83]	0.480	−0.392	97 ± 62	[88]
0.100	−0.095	69 ± 12	[83]	0.570	−0.451	100.3 ± 3.7	[85]
0.120	−0.113	68.6 ± 26.2	[82]	0.593	−0.465	104 ± 13	[84]
0.170	−0.157	83 ± 8	[83]	0.600	−0.470	87.9 ± 6.1	[86]
0.179	−0.164	75 ± 4	[84]	0.680	−0.518	92 ± 8	[84]
0.199	−0.181	75 ± 5	[84]	0.730	−0.548	97.3 ± 7	[86]
0.200	−0.182	72.9 ± 29.6	[82]	0.781	−0.577	105 ± 12	[84]
0.270	−0.239	77 ± 14	[83]	0.875	−0.628	125 ± 17	[84]
0.280	−0.246	88.8 ± 36.6	[82]	0.880	−0.631	90 ± 40	[88]
0.320	−0.277	79.2 ± 5.6	[85]	0.900	−0.641	117 ± 23	[83]
0.352	−0.301	83 ± 14	[84]	1.037	−0.711	154 ± 20	[84]
0.3802	−0.322	83 ± 13.5	[84]	1.300	−0.832	168 ± 17	[83]
0.400	−0.336	95 ± 17	[83]	1.363	−0.859	160 ± 33.6	[89]
0.4004	−0.336	77 ± 10.2	[84]	1.430	−0.887	177 ± 18	[83]
0.4247	−0.353	87.1 ± 11.2	[84]	1.530	−0.928	140 ± 14	[83]
0.440	−0.364	82.6 ± 7.8	[86]	1.750	−1.011	202 ± 40	[83]
0.4497	−0.371	92.8 ± 12.9	[84]	1.965	−1.086	186.5 ± 50.4	[89]
0.470	−0.385	89 ± 34	[87]	2.340	−1.205	222 ± 7	[90]
				2.360	−1.211	226 ± 8	[91]

References

1. Riess, Adam G., et al.: Observational evidence from supernovae for an accelerating universe and a cosmological constant. Astron. J. **116**, 1009–1038 (1998)
2. Perlmutter, S., et al.: Measurements of Ω and Λ from 42 high redshift supernovae. Astrophys. J. **517**, 565–586 (1999)
3. Meszaros, Attila: On the Reality of the accelerating universe. Astrophys. J. **580**, 12–15 (2002)
4. Arnaud, M.: et al. Planck intermediate results. XXXI. Microwave survey of Galactic supernova remnants. Astron. Astrophys., 586:A134, (2016)
5. Ahn, Christopher P., Alexandroff, Rachael, Prieto, Carlos Allende, Anderson, Scott F., Anderton, Timothy, Andrews, Brett H., Aubourg, Éric., Bailey, Stephen, Balbinot, Eduardo, Barnes, Rory, et al.: The ninth data release of the sloan digital sky survey: first spectroscopic data from the sdss-iii baryon oscillation spectroscopic survey. Astrophys. J. Suppl. Seri. **203**(2), 21 (2012)
6. Padmanabhan, T.: Dark energy: mystery of the millennium. In AIP Conference Proceedings, volume 861, pages 179–196. American Institute of Physics, (2006)
7. Aghanim, N.: et al. Planck 2018 results. VI. Cosmological parameters. Astron. Astrophys., 641:A6, 2020. [Erratum: Astron.Astrophys. 652, C4 (2021)]
8. Alam, Shadab, Ata, Metin, Bailey, Stephen, Beutler, Florian, Bizyaev, Dmitry, Blazek, Jonathan A., Bolton, Adam S., Brownstein, Joel R., Burden, Angela, Chuang, Chia-Hsun., et al.: The clustering of galaxies in the completed sdss-iii baryon oscillation spectroscopic survey: cosmological analysis of the dr12 galaxy sample. Mon. Not. R. Astron. Soc. **470**(3), 2617–2652 (2017)
9. Florian, Beutler, Chris, Blake, Matthew, Colless, Jones, D.: Heath, Staveley-Smith Lister, Campbell Lachlan, Parker Quentin, Saunders Will, Watson Fred: The 6df galaxy survey: baryon acoustic oscillations and the local hubble constant. Mon. Noti. R. Astron. Soc **416**(4), 3017–3032 (2011)
10. Alam Shadab, Aubert Marie, Avila Santiago, Balland Christophe, Bautista Julian E., Bershady Matthew A., Bizyaev Dmitry, Blanton Michael R., Bolton Adam S., Bovy Jo, et al. Completed sdss-iv extended baryon oscillation spectroscopic survey: Cosmological implications from two decades of spectroscopic surveys at the apache point observatory. Physical Review D, 103(8), (2021)
11. Abbott, T.M.C., et al.: Dark Energy Survey year 1 results: Cosmological constraints from galaxy clustering and weak lensing. Phys. Rev. D **98**(4), 043526 (2018)
12. Macaulay, E., et al.: First Cosmological Results using Type Ia Supernovae from the Dark Energy Survey: Measurement of the Hubble Constant. Mon. Not. Roy. Astron. Soc. **486**(2), 2184–2196 (2019)
13. Krause, E.: et al. Dark Energy Survey Year 1 Results: Multi-Probe Methodology and Simulated Likelihood Analyses. 6 (2017)
14. Riess, Adam G., Casertano, Stefano, Yuan, Wenlong, Macri, Lucas M., Scolnic, Dan: Large magellanic cloud cepheid standards provide a 1% foundation for the determination of the hubble constant and stronger evidence for physics beyond λcdm. Astrophys. J. **876**(1), 85 (2019)
15. Kenneth C. Wong et al. H0LiCOW – XIII. A 2.4 percent measurement of H0 from lensed quasars: 5.3σ tension between early- and late-Universe probes. Mon. Not. Roy. Astron. Soc., 498(1):1420–1439, (2020)
16. Riess, Adam G., Breuval Louise, Yuan Wenlong, Casertano Stefano, Macri Lucas M., Bradley Bowers J., Scolnic Dan, Cantat-Gaudin Tristan, Anderson Richard I., Reyes Mauricio Cruz.: Cluster cepheids with high precision gaia parallaxes, low zero-point uncertainties, and hubble space telescope photometry. The Astrophysical Journal, 938(1):36, oct (2022)
17. Amendola Luca, Tsujikawa Shinji.: Dark energy: theory and observations. Cambridge University Press, (2010)

18. Bamba, Kazuharu, Capozziello, Salvatore, Nojiri, Shin'ichi, Odintsov, Sergei D.: Dark energy cosmology: the equivalent description via different theoretical models and cosmography tests. Astrophys. Space Sci. **342**, 155–228 (2012)
19. Copeland Edmund, J., Mohammad, Sami, Shinji, Tsujikawa: Dynamics of dark energy. Int. J. Modern Phys. D. **15**(11), 1753–1935 (2006)
20. Peebles, P.J.E., Ratra, B.: Quintessence: A review. Rev. Mod. Phys. **75**(2), 559–606 (2003)
21. Armendariz-Picon, C., Mukhanov, V., Steinhardt, P.J.: k-essence as a model for dark energy. Phys. Rev. Lett. **85**(15), 4438–4441 (2001)
22. Roy, Nandan, Goswami, Sangita, Das, Sudipta: Quintessence or phantom: study of scalar field dark energy models through a general parametrization of the hubble parameter. Phys. Dark Univ. **36**, 101037 (2022)
23. Banerjee Aritra, Cai Haiying, Heisenberg Lavinia, Eoin Ó. Colgáin, M. M. Sheikh-Jabbari, and Tao Yang. Hubble sinks in the low-redshift swampland. Phys. Rev. D, 103(8):L081305, (2021)
24. Lee Bum-Hoon, Lee Wonwoo, Eoin Ó. Colgáin, M. M. Sheikh-Jabbari, and Somyadip Thakur. Is local H_0 at odds with dark energy EFT? JCAP, 04(04):004, (2022)
25. Krishnan, C., Ó. Colgáin, E., Sheikh-Jabbari, M. M., Yang Tao.: Running Hubble Tension and a H0 Diagnostic. Phys. Rev. D, 103(10):103509, (2021)
26. Roy, Nandan: Exploring the possibility of interacting quintessence model as an alternative to the ΛCDM model. Gen. Rel. Grav. **55**(10), 115 (2023)
27. Nandan Roy and L. Arturo Ureña López. Tracker behaviour of quintom dark energy and the Hubble tension. 12 2023
28. Adame, A. G.: et al. DESI 2024 VI: Cosmological Constraints from the Measurements of Baryon Acoustic Oscillations. 4 (2024)
29. Calderon, R.: et al. DESI 2024: Reconstructing Dark Energy using Crossing Statistics with DESI DR1 BAO data. 5 (2024)
30. Roy, Nandan, Goswami, Sangita, Das, Sudipta: Quintessence or phantom: Study of scalar field dark energy models through a general parametrization of the Hubble parameter. Phys. Dark Univ. **36**, 101037 (2022)
31. Nandan Roy. Dynamical dark energy in the light of DESI 2024 data. 6 (2024)
32. Dinda, Bikash R.: A new diagnostic for the null test of dynamical dark energy in light of DESI 2024 and other BAO data. JCAP **09**, 062 (2024)
33. Dinda, Bikash R., Maartens, Roy.: Model-agnostic assessment of dark energy after DESI DR1 BAO. 7 (2024)
34. Francisco X. Linares Cedeño, Nandan Roy, and L. Arturo Ureña López. Tracker phantom field and a cosmological constant: Dynamics of a composite dark energy model. Phys. Rev. D, 104(12):123502, (2021)
35. Sen, Anjan A., Adil, Shahnawaz A., Sen, Somasri: Do cosmological observations allow a negative Λ? Mon. Not. Roy. Astron. Soc. **518**(1), 1098–1105 (2022)
36. Alberto Vázquez, J., Tamayo David, Garcia-Arroyo Gabriela, Gómez-Vargas Isidro, Quiros Israel, Sen Anjan A.: Coupled multiscalar field dark energy. Phys. Rev. D, 109(2):023511, (2024)
37. Adil, Shahnawaz A., Mukhopadhyay, Upala, Sen, Anjan A., Vagnozzi, Sunny: Dark energy in light of the early JWST observations: case for a negative cosmological constant? JCAP **10**, 072 (2023)
38. Cai, Yi.-Fu., Saridakis, Emmanuel N., Setare, Mohammad R., Xia, Jun-Qing.: Quintom Cosmology: Theoretical implications and observations. Phys. Rept. **493**, 1–60 (2010)
39. Burd, A.B., Barrow, John D.: Inflationary models with exponential potentials. Nuclear Physics B, 308(4):929–945, (1988)
40. Peebles, P. J. E., Ratra Bharat.: Cosmology with a Time-Variable Cosmological "Constant". The Astrophysical Journal Letters, 325:L17, February (1988)
41. Barrow, John D., Parsons, Paul: Inflationary models with logarithmic potentials. Physical Review D **52**(10), 5576–5587 (1995)
42. Parsons, Paul, Barrow, John D.: Generalized scalar field potentials and inflation. Physical Review D **51**(12), 6757–6763 (1995)
43. Sahni, Varun, Wang, Limin: New cosmological model of quintessence and dark matter. Phys. Rev. D **62**, 103517 (2000)
44. Gong, Yungui, Wang, Anzhong, Zhang, Yuan-Zhong.: Exact scaling solutions and fixed points for general scalar field. Phys. Lett. B **636**(5), 286–292 (2006)

45. VARUN SAHNI and ALEXEI STAROBINSKY: The case for a positive cosmological $\bigwedge$-term. Int. J. Modern Phys. D **09**(04), 373–443 (2000)

46. James E. Lidsey, Tonatiuh Matos, and L. Arturo Ureña-López. Inflaton field as self-interacting dark matter in the braneworld scenario. Physical Review D, 66(2), (2002)

47. Tonatiuh Matos and L Arturo Ureña-López. Quintessence and scalar dark matter in the universe. Classical and Quantum Gravity, 17(13):L75-L81, (2000)

48. L. Arturo Ureña-López and Tonatiuh Matos. New cosmological tracker solution for quintessence. Physical Review D, 62(8), (2000)

49. Tonatiuh Matos, José-Rubén Luévano, Israel Quiros, L. Arturo Ureña-López, and José Alberto Vázquez. Dynamics of scalar field dark matter with a cosh-like potential. Physical Review D, 80(12), (2009)

50. Yoelsy Leyva, Dania González, Tamé González, Tonatiuh Matos, and Israel Quiros. Dynamics of a self-interacting scalar field trapped in the braneworld for a wide variety of self-interaction potentials. Physical Review D, 80(4), (2009)

51. Leon, Genly: On the past asymptotic dynamics of non-minimally coupled dark energy. Class. Quantum Gravity **26**(3), 035008 (2009)

52. Aref'eva, I.. Ya.., Bulatov, N.V., Vernov, SYu.: Stable exact solutions in cosmological models with two scalar fields. Theor. Math. Phys. **163**(3), 788–803 (2010)

53. Dagoberto Escobar, Carlos R Fadragas, Genly Leon, and Yoelsy Leyva. Phase space analysis of quintessence fields trapped in a randall-sundrum braneworld: a refined study. Classical and Quantum Gravity, 29(17):175005,(2012)

54. Dagoberto Escobar, Carlos R Fadragas, Genly Leon, and Yoelsy Leyva. Phase space analysis of quintessence fields trapped in a randall-sundrum braneworld: anisotropic bianchi i brane with a positive dark radiation term. Classical and Quantum Gravity, 29(17):175006, (2012)

55. Sergio del Campo, Carlos R. Fadragas, Ramón Herrera, Carlos Leiva, Genly Leon, and Joel Saavedra. Thawing models in the presence of a generalized chaplygin gas. Physical Review D, 88(2), (2013)

56. Dagoberto Escobar, Carlos de la Caridad Rodriguez Fadragas, Genly Leon, and Yoelsy Leyva. Phase space analysis of quintessence fields trapped in a randall-sundrum braneworld: anisotropic bianchi i brane with a negative dark radiation term. 01 (2013)

57. Fadragas Carlos R, Leon Genly, Saridakis Emmanuel N.: Dynamical analysis of anisotropic scalar-field cosmologies for a wide range of potentials. Classical and Quantum Gravity, 31(7):075018, (2014)

58. Leon Genly, Leyva Yoelsy, Socorro, J.: Quintom phase-space: beyond the exponential potential, (2013)

59. Leon Genly, Paliathanasis Andronikos, Morales-Martínez, Jorge Luis.: The past and future dynamics of quintom dark energy models. The European Physical Journal C, 78(9), (2018)

60. Genly Leon, Saikat Chakraborty, Sayantan Ghosh, Raja Solanki, P.K. Sahoo, and Esteban González. Scalar field evolution at background and perturbation levels for a broad class of potentials. Fortschritte der Physik, 71(10-11), (2023)

61. Cid, Antonella, Leon, Genly, Leyva, Yoelsy: Intermediate accelerated solutions as generic late-time attractors in a modified jordan-brans-dicke theory. J. Cosmol. Astropart. Phys. **2016**(02), 027–027 (2016)

62. Paliathanasis, Andronikos, Pan, Supriya, Pramanik, Souvik: Scalar field cosmology modified by the generalized uncertainty principle. Class. Quantum Gravity **32**(24), 245006 (2015)

63. Savaş Arapoğlu, A., Emrah Yükselci, A.: Dynamical system analysis of quintessence models with exponential potential - revisited. Modern Physics Letters A, 34(09):1950069, (2019)

64. Bahamonde, Sebastian, Böhmer, Christian G., Carloni, Sante, Copeland, Edmund J., Fang, Wei, Tamanini, Nicola: Dynamical systems applied to cosmology: Dark energy and modified gravity. Phys. Rep. **775–777**, 1–122 (2018)

65. Quiros, Israel: Selected topics in scalar-tensor theories and beyond. International Journal of Modern Physics D **28**(07), 1930012 (2019)

66. Genly Leon , Andronikos Paliathanasis. Extended phase-space analysis of the hořava-lifshitz cosmology. The European Physical Journal C, 79(9), (2019)

67. Leon, Genly, Silva, Felipe Orlando Franz.: Generalized scalar field cosmologies: a global dynamical systems formulation. Class. Quantum Gravity **38**(1), 015004 (2020)

68. Leon, Genly, Silva, Felipe Orlando Franz.: Generalized scalar field cosmologies: theorems on asymptotic behavior. Class. Quantum Gravity **37**(24), 245005 (2020)

69. Patrocinio Pérez, Ulises Nucamendi, and Roberto De Arcia. Revisiting dynamics of interacting quintessence. The European Physical Journal C, 81(12), (2021)

70. Wompherdeiki Khyllep, Jibitesh Dutta, Spyros Basilakos, and Emmanuel N. Saridakis. Background evolution and growth of structures in interacting dark energy scenarios through dynamical system analysis. Physical Review D, 105(4), (2022)
71. Sujoy Bhanja, Goutam Mandal, Abdulla Al Mamon, Sujay Kr. Biswas. Dynamical systems analysis of an interacting scalar field model in an anisotropic universe. Journal of Cosmology and Astroparticle Physics, 2023(10):050, (2023)
72. Sudip Halder, S. D. Odintsov, Supriya Pan, Tapan Saha, and Emmanuel N. Saridakis. Interacting phantom dark energy: new accelerating scaling attractors, (2024)
73. Andronikos Paliathanasis, Amlan Halder, Genly Leon. Revise the dark matter-phantom scalar field interaction, (2024)
74. Roy, Nandan, Bhadra, Nivedita: Dynamical systems analysis of phantom dark energy models. JCAP **1806**, 002 (2018)
75. Nandan Roy, Alma X. Gonzalez-Morales, and L. Arturo Urena-Lopez. New general parametrization of quintessence fields and its observational constraints. Phys. Rev., D98(6):063530, (2018)
76. Edmund J. Copeland, Adam Moss, Sergio Sevillano Muñoz, and Jade M.M. White. Scaling solutions as early dark energy resolutions to the hubble tension. Journal of Cosmology and Astroparticle Physics, 2024(05):078, (2024)
77. Ramadan, Omar F., Karwal, Tanvi, Sakstein, Jeremy: Attractive proposal for resolving the Hubble tension: Dynamical attractors that unify early and late dark energy. Phys. Rev. D **109**(6), 063525 (2024)
78. Roy, Nandan, Banerjee, Narayan: Quintessence Scalar Field: A Dynamical Systems Study. Eur. Phys. J. Plus **129**, 162 (2014)
79. Roy, Nandan, Banerjee, Narayan: Tracking quintessence: a dynamical systems study. Gen. Rel. Grav. **46**, 1651 (2014)
80. Roy, Nandan, Banerjee, Narayan: Dynamical systems study of Chameleon scalar field. Annals Phys. **356**, 452–466 (2015)
81. Roy, Nandan, Banerjee, Narayan: Generalized Brans-Dicke Theory: A Dynamical Systems Analysis. Phys. Rev. D **95**(6), 064048 (2017)
82. Cong, Zhang, Han, Zhang, Shuo, Yuan, Siqi, Liu, Tong-Jie, Zhang, Yan-Chun, Sun: Four new observational h(z) data from luminous red galaxies in the sloan digital sky survey data release seven. Res. Astron. Astrophys. **14**(10), 1221 (2014)
83. Simon, Joan, Verde, Licia, Jimenez, Raul: Constraints on the redshift dependence of the dark energy potential. Phys. Rev. D **71**, 123001 (2005)
84. Moresco, M., Cimatti, A., Jimenez, R., Pozzetti, L., Zamorani, G., Bolzonella, M., Dunlop, J., Lamareille, F., Mignoli, M., Pearce, H., Rosati, P., Stern, D., Verde, L., Zucca, E., Carollo, C.M., Contini, T., Kneib, J.-P., Le Fè vre, O., Lilly, S.J., Mainieri, V., Renzini, A., Scodeggio, M., Balestra, I., Gobat, R., McLure, R., Bardelli, S., Bongiorno, A., Caputi, K., Cucciati, O., de la Torre, S., de Ravel, L., Franzetti, P., Garilli, B., Iovino, A., Kampczyk, Knobel, P C., Kovač, K., Le Borgne, J.-F., Le Brun, V., Maier, C., Pelló, R., Peng, Y., Perez-Montero, E., Presotto, V., Silverman, J.D., Tanaka, M., Tasca, L.A.M., Tresse, L., Vergani, D., Almaini, O., Barnes, L., Bordoloi, R., Bradshaw, E., Cappi, A., Chuter, R., Cirasuolo, M., Coppa, G., Diener, C., Foucaud, S., Hartley, W., Kamionkowski, M., Koekemoer, A.M., López-Sanjuan, C., McCracken, H.J., Nair, P., Oesch, P., Stanford, A., Welikala, N.: Improved constraints on the expansion rate of the universe up to z 1.1 from the spectroscopic evolution of cosmic chronometers. Journal of Cosmology and Astroparticle Physics, 2012(08):006–006, (2012)
85. Cuesta, Antonio J., et al.: The clustering of galaxies in the SDSS-III Baryon Oscillation Spectroscopic Survey: Baryon Acoustic Oscillations in the correlation function of LOWZ and CMASS galaxies in Data Release 12. Mon. Not. Roy. Astron. Soc. **457**(2), 1770–1785 (2016)
86. Blake, Chris, et al.: The WiggleZ Dark Energy Survey: Joint measurements of the expansion and growth history at z < 1. Mon. Not. Roy. Astron. Soc. **425**, 405–414 (2012)
87. Ratsimbazafy, A.L., Loubser, S.I., Crawford, S.M., Cress, C.M., Bassett, B.A., Nichol, R.C., Väisänen, P.: Age-dating Luminous Red Galaxies observed with the Southern African Large Telescope. Mon. Not. Roy. Astron. Soc. **467**(3), 3239–3254 (2017)
88. Stern Daniel , Jimenez Raul, Verde Licia, Kamionkowski Marc, Stanford S. Adam.: Cosmic Chronometers: Constraining the Equation of State of Dark Energy. I: H(z) Measurements. JCAP, 02:008, (2010)
89. Moresco, Michele: Raising the bar: new constraints on the Hubble parameter with cosmic chronometers at z ∼ 2. Mon. Not. Roy. Astron. Soc. **450**(1), L16–L20 (2015)

90. Delubac, Timothée, et al.: Baryon acoustic oscillations in the Lyα forest of BOSS DR11 quasars. Astron. Astrophys. **574**, A59 (2015)
91. Blomqvist, Michael, et al.: Broadband distortion modeling in Lyman-α forest BAO fitting. JCAP **11**, 034 (2015)